RESEARCH ARTICLE   **Open Access**

First evaluation of a novel ionisation chamber for thermal neutron beam monitoring

Vendula Maulerová[1,2,3,4], Kalliopi Kanaki[1*], Martin Klein[5], Christian J. Schmidt[5,6], Peter M. Kadletz[1,10], Alessio Laloni[1] and Richard J. Hall-Wilton[1,7,8,9]

*Correspondence:
kalliopikanaki@gmail.com
[1] European Spallation Source ERIC,
22100, Lund, Sweden
Full list of author information is
available at the end of the article

Abstract

The European Spallation Source ERIC (ESS), currently under construction in Lund, Sweden is a facility established to deliver the highest integrated neutron flux originating from a pulsed source with the aim of supporting an initial fifteen neutron instruments for cutting edge science experiments. This in turn requires reliable monitoring at complex neutron beam lines: in particular, linearity, timing capability, adaptability of the design for various flux ranges (dynamic range) and sensitivity to neutrons within the range of 0.6-10Å are expected from the neutron beam monitors to be installed at the ESS beam lines. Additionally, operational stability and low attenuation are also desirable characteristics for such neutron beam monitoring. A prototype neutron beam monitor based on the ionisation chamber principle and a boron converter, designed by CDT CASCADE Detector Technologies GmbH and ESS, has been investigated at the BER-II research reactor of Helmholtz Zentrum Berlin (HZB). The effort to design and investigate a thermal neutron ionisation beam monitor was initiated by adapting the concept of ionisation chambers previously known elsewhere. So far all the characterised neutron beam monitors discriminate neutron hits on a discrete event basis (pulse mode), whereas the beam monitor prototype introduced in this paper estimates the total flux as a function of current (current mode). While most other neutron beam monitoring devices and detectors rely upon a signal amplifying gain stage, the ionisation chamber operates without any gain and is consequently robust against typical detector ageing effects that compromise the sensitivity over time. The initial tests were performed at the ESS V20 test beam line under realistic conditions resembling those of the future pulses of ESS. The linearity is demonstrated for 3Å pulses in the flux range of 2-3 $\times$ 10^5 n/s/cm^2 and for white pulses (0.6-10Å) in the range of 1-5 $\times$ 10^6 n/s/cm^2. The timing behaviour resembles the data previously recorded at the V20 beam lines. This novel implementation of a neutron sensitive ionisation chamber shows great promise for beam monitoring and diagnostics at ESS. As the ionisation beam monitor itself is an entirely passive device, it is adequately robust to be employed in areas of high irradiation where no regular servicing or maintenance can be provided.

Keywords: Ionisation chamber; Thermal neutron; Neutron monitor

1 Introduction

The purpose of neutron beam monitors is to sample the neutron beam whilst leaving it essentially unperturbed. Thermal neutron beam monitors are neutron detectors with low efficiency (10^{-6}-10^{-2}) and preferably low attenuation. Only a low fraction (typically < 5%) of neutrons is scattered/absorbed and an even lower fraction is subsequently detected, which ensures that the neutron beam is left undisturbed for further purposes. Neutron beam monitors can be permanently or temporarily placed in the neutron beam lines in order to characterise moderator performance and in-monolith optics, perform chopper diagnostics, spectral normalisation, transmission measurements and calibration of flight paths [1]. Typically neutron detectors and neutron beam monitors are discrete-event based detectors: when a neutron hits the detector converter (^{10}B, ^6Li, ^2N, $^{235}UO_2$ or ^3He [2–4] are often used as converters for thermal neutrons), charged ions are released, which by subsequent processes trigger an electronic system and a pulse is produced. For an appropriate energy threshold this pulse corresponds to a single neutron hit. The neutron energy is not directly measured and must be obtained via the concept of the time-of-flight (TOF) [5]. In contrast, high energy particle accelerators typically utilise ionisation chambers for beam loss monitoring.

This paper, however, presents the possibility of measuring the neutron beam flux, instead of with the identification of discrete events, by measuring the current by integrating the charge generated by the interaction of the chamber with the neutron beam in discrete time intervals.This concept has been well characterised for charged particles and γ-rays [6, 7] and ESS plans to deploy several ionisation chambers to monitor the beam loss at the LINAC proton beam accelerator [8, 9]. By selecting the appropriate neutron converter, the concept can have a suitable utilisation for thermal neutron beam characterisation as well.

The ESS [10–12] is established to design, construct, commission and operate a multidisciplinary research facility based around a neutron source with unique properties, enabling in turn scientific discoveries in its planned fifteen instrument stations [13]. The uniqueness of the source lies in neutrons produced from an accelerated proton beam collisions in a rotating Tungsten target, delivered in 2.86 ms long pulses at the frequency of 14 Hz. The neutron flux at its peak will be approximately 30 times higher than the flux from any reactor source and 5 times higher than the flux from any other currently operational spallation source [10]. The described pulse structure in addition with the possibility for bispectral (thermal and cold neutrons) extraction from the neutron moderators [14, 15] allows for the use of beams with rates and a range of neutron wavelengths that will be unprecedented when ESS reaches its foreseen operational power. The unique long pulse structure will be present even for initial operations at ESS with low power. Subsequently, new possibilities for the experimental research in material sciences are envisioned [16–19].

The range of wavelengths transported to the instrument sample position runs from 0.6Å to ca. 15-20Å. The lower limit is given by the constraints of neutron transport through curved waveguides [20], while the upper limit by the difficulty in transporting ultra-cold neutrons. A number of beam monitors [2] are to be placed along the beam lines for the various use cases mentioned earlier. The multitude and complexity of the ESS beam line components, much higher than in existing neutron sources, imply a greater need for monitoring. Therefore, aside from previously characterised beam monitors [2, 3, 21–27] based on discrete events, the concept of an ionisation chamber with a boron converter produc-
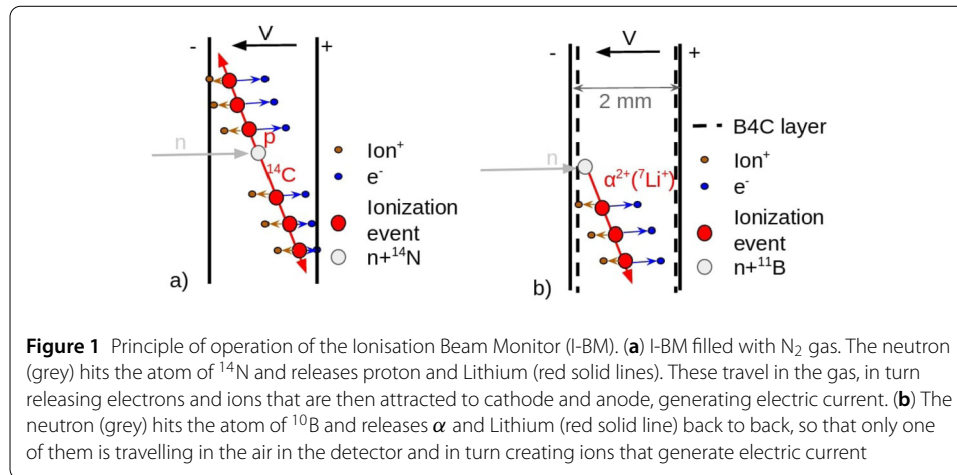
ing continuous current has been suggested as a candidate for the location close to the so-called bunker, a shielding block surrounding the target monolith that hosts the extraction and primary optical transport guides and in some occasions even chopper systems [28]. At least one beam monitor per instrument is foreseen to be placed inside the bunker zone. A desirable characteristic for the monitors in these locations is also to perform quasi-parasitically, i.e. by minimisation of the material in the beam, the beam would be left almost undisturbed. This work describes the principle of an operation of such an ionisation chamber, the specific design used for the V20 beam line tests, the experimental procedure and its results, and finally it suggests the optimisation for the design for high neutron flux fields based on variable parameters.

2 Principle of operation

Ionisation chambers are widely use to monitor beam energy losses and therefore used for beam monitoring in high flux and low flux environments in general—an example can be beam loss monitoring [29–31]. The losses from high energy proton beams are large particle showers, including all particle species and the resulting detected signal is a combination of all of these. The dominant component depends on the location of these beam monitors. Often the signal is dominated by signals from γ or fast neutrons [32, 33]. Similar principles, but based on diamond detectors, are also used for beam loss monitors at the experiments at the Large Hadron Collider at CERN [34]. Ionisation chambers can be used in both event mode and continuous current mode. The concept of an ionisation chamber operating in current mode is a concept known for more than half a century in the field of particle physics and dosimetry [35]. The event mode, widely used in general [21], produces a pulse with each particle event. The continuous current mode, subject of this article, delivers charge continuously which is proportional to the intensity of the incoming beam of particles and is suitable for high flux environments. For high rates, recording each pulse individually becomes a challenge for the detector electronics and can lead to pileup: many pulses arriving at the same time. The current mode on the other hand continuously produces current that corresponds to the flux of neutrons. With a dedicated electronic shielding, current mode can achieve capability to measure both low flux and high flux beams: very small signals can be measured too down to the detection of individual neutrons [36].

The accelerator group at ESS is using a new type of neutron beam loss monitor based on gaseous Micromegas detectors with a polyethylene moderator that thermalises neutrons, designed to be sensitive to fast neutrons and with little sensitivity to photons [37, 38]. The transition between pulse and current mode is automatic in this detector. When pileup occurs, the readout changes from extracting neutron rates via counting (counts per μs) to extracting counts via charge (event charge divided by average charge for single neutron). The transition is based on a threshold setting on pulse duration. It continuously reports counts in an 1 μs window [39, 40]. Current mode based electronics can be applied even for other commercially available detectors such as ^{3}He and BF$_3$ proportional counters [41].

Figure 1 depicts two examples of an ionisation chamber for neutron beam monitoring. Figure 1(a) shows an ionisation chamber filled with nitrogen (N$_2$). The incoming neutron interacts with the nitrogen nucleus and depending on the neutron energy, two reactions can occur. For thermal neutrons: ^{14}N+n $\longrightarrow$ ^{14}C+p+625.89 keV and for fast neutrons: ^{14}N+n $\longrightarrow$ ^{11}B+α-158 keV. The cross section for the thermal neutron (1.8Å) capture reaction with nitrogen is 1.83 b [42]. The efficiency is a function of the N$_2$ pressure: the

Figure 1 Principle of operation of the Ionisation Beam Monitor (I-BM). (**a**) I-BM filled with N_2 gas. The neutron (grey) hits the atom of ^{14}N and releases proton and Lithium (red solid lines). These travel in the gas, in turn releasing electrons and ions that are then attracted to cathode and anode, generating electric current. (**b**) The neutron (grey) hits the atom of ^{10}B and releases α and Lithium (red solid line) back to back, so that only one of them is travelling in the air in the detector and in turn creating ions that generate electric current

number of converted neutrons depends on the density of the gas as well as the mean free path and cross section for the respective incident neutron energy.

Figure 1(b) shows an ionisation chamber filled with air of room temperature and a boron coating B_4C on both electrodes. When the incoming neutron hits the boron, two reactions can occur: $^{10}B+n \longrightarrow {}^7Li^*+\alpha \longrightarrow {}^7Li+\alpha + \gamma(0.48 \text{ MeV})+ 2.31$ MeV (94% of the time), $^{10}B+n \longrightarrow {}^7Li+\alpha + 2.79$ MeV (6% of the time). The cross section for the neutron capture reaction of ^{10}B for thermal neutrons is 3840 b [43]. For two layers of 2.93 μm of B_4C deposited on 100 μm thick aluminium cathodes, the conversion efficiency is 7.74% (calculated with [44, 45]). Only part of the α and ^7Li ionising energy is deposited, as the mean free path of the α particle in air ca. 4 cm. For the I-BM (SN001) (with a gap between the chambers of 2 mm), the mean energy deposit amounts to 410 keV, resulting in $Q_0 = 24000e^-$ per converted neutron.

In order to distinguish the neutron signal from γ-ray signal, a system of two ionisation chambers is introduced. There is a neutron sensitive ionisation chamber (one with a neutron converter) and a reference chamber. If the reference chamber produces the same signal as the neutron sensitive chamber, the event is considered a background or γ event. In terms of the design, the CDT I-BM (shown in Fig. 2) consists of two parallel round disc capacitors with a gap of 2.0 mm, i.e. two chambers sharing a common high voltage (HV) electrode. One of the chambers is neutron sensitive, coated with $(2 \times 2.92 \pm 0.05)$ μm thick, 97% enriched $^{10}B_4C$ layer. Note that this thickness is optimised for maximum efficiency for the purposes of simplifying testing the monitor. It does not represent an optimised configuration for an operational monitor. The outside electrodes (signal electrodes) have an active diameter of 70 mm and a thickness of 100 μm.

3 Design

The detector housing of the monitor is made of aluminium with the entrance windows being 100 μm thick. The chambers are isolated from the housing and connected via the two signal electrodes to a noise and bandwidth optimised Transimpedance amplifier (TIA). The signal cable has been designed as an ultra-low capacitance cable in order to perform with the lowest possible noise. The schematic representation of the I-BM readout is presented in Fig. 3. As the HV electrode is sandwiched between the two chambers, the neutron signal is fed to an inverting input, while the signal from the reference cell is fed to a
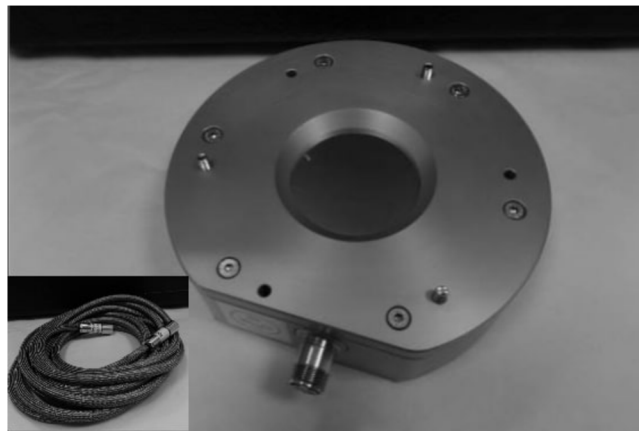
Figure 2 The CDT I-BM together with its ultra-low capacitance cables. The diameter of the whole monitor is ca. 20 cm and the sensitive area diameter is 70 mm
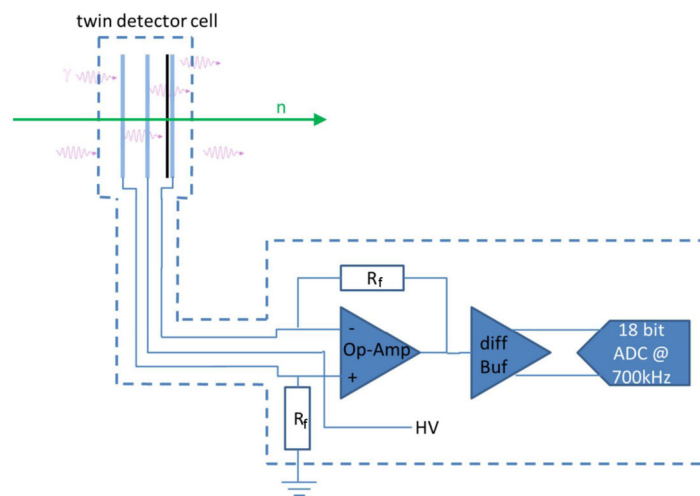
Figure 3 Schematic representation of the I-BM readout concept. The symmetric parallel plate ionisation chamber pair on the left is fed with a biasing voltage on its central electrode. One of the chambers is boron coated. γ-induced signals together with noise are annihilated while the neutron signal is read out by a noise-optimised TIA, limited in bandwidth to about 125 kHz. In the final design the bandwidth is actually limited to 50 kHz, precisely the bandwidth needed to detect a Gaussian pulse of 10μs FWHM

non-inverting input. Since both current signals are fed through the same impedance, in case the signals are the same in the neutron and the reference chambers, the total signal is zeroed. It is the differential signal that acts as the total output of the TIA.

The relation between the neutron flux, Φ_c, and the current (I_{monitor})/voltage ($U_{\text{out–TIA}}$) is given by equation (2), where ϵ_n is a detection efficiency for the coating thickness of 2.93 μm layer on both cathodes with 97% of boron enrichment, $Q_0 = 24000e^-$ is the ratio of generated electrons per converted neutron for a 2.0 mm gap, 2/3 is a factor related to humidity. I_{monitor} is the differential current measured as an output in units of A and U_{out}

Figure 4 Efficiency of boron coating used as a function of wavelength from [45]
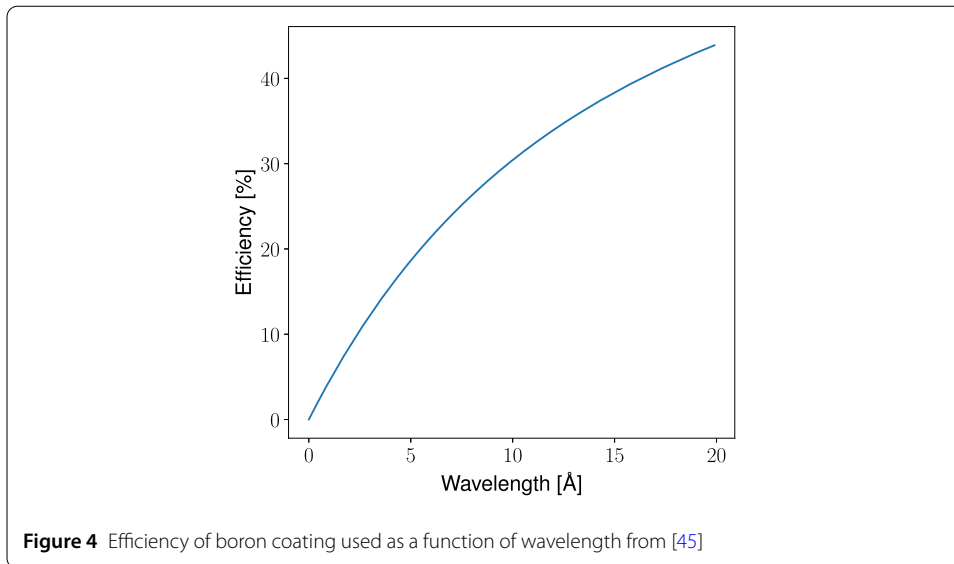
is the corresponding voltage.

$$\Phi_c = \frac{I_{\text{monitor}}}{Q_0 \epsilon_n \cdot \frac{2}{3}} = 3.8 \cdot 10^{14} \frac{1}{s} I_{\text{monitor}}[A] \tag{1}$$
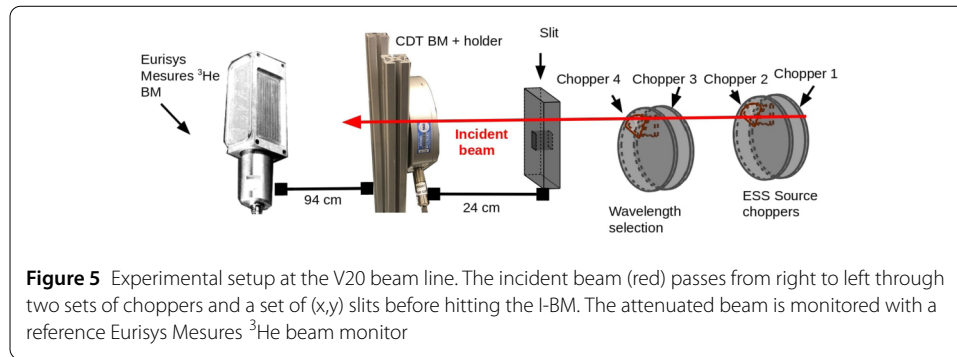
$$= 1.3 \cdot 10^8 \frac{1}{s} U_{\text{out}}[V]. \tag{2}$$

The detection efficiency of the boron coating used in this detector as a function of wavelength is shown in Fig. 4. This thickness was chosen in order to perform the initial measurements at V20, where flux is relatively low compared to the envisioned flux in the ESS bunker zone. For later models of the detector the boron layers are expected to be much thinner (e.g. 100 nm of enriched B_4C) in order to optimise the detection efficiency with respect to the neutron flux.

As described above, the signal from the reference chamber is subtracted from the signal from the neutron sensitive chamber and the common differential signal is then optimised in a TIA through the choice of input amplifier, feedback resistor, input capacitance (sensor and cable) and compensation capacitance. The TIA is connected to a computer via a USB cable and a dedicated data acquisition is used. When the time-stamping frequency ω is set for the highest time resolution option, the data readout stores an ADC value every 100 ns. The frequency of time-stamping can be set in units of $100 \cdot 2^k$ where k is a positive integer from 0 to 15, i.e. the resolution can be set from 30.5 kHz to 10 MHz. The ADC value can then be converted to units of voltage U or current I, where $U = RI$ with a circuit resistance of $R = 3\Omega$. The *.emd* data output format stores the ADC values in a form of a float number while the TTL signal and the control of the data loss are stored in the form of a hexadecimal counter. Clocks are reset every $2^{13} \cdot \omega$ ns, i.e. at 100 ns ≈ 0.8192 s.

4 V20 beam line

The V20 beam line at HZB was designed to emulate the planned ESS pulse structure using two counter-rotating double-disk chopper systems [46], that can deliver a 2.86 ms pulse length with a repetition rate of 14 Hz. However, the flexible design of V20 offers convenient

Figure 5 Experimental setup at the V20 beam line. The incident beam (red) passes from right to left through two sets of choppers and a set of (x,y) slits before hitting the I-BM. The attenuated beam is monitored with a reference Eurisys Mesures ^{3}He beam monitor

control of both the flux and wavelength range of the neutron beam. The full extent of the choppers and variable settings are discussed in [47].

In this work, the two double-disk choppers, source choppers (SC) and wavelength band (WB) choppers, were used in both counter-rotation and co-rotation mode. These choppers were earlier commissioned for ESS timing requirements [1]. The SCs were used to modify the time structure of the pulse and therefore the incoming flux. For additional measurements, the WB choppers were used to narrow the wavelength band, in order to restrict it to a selection around 3.0Å.

Figure 5 illustrates the experimental setup for the I-BM test. The neutron beam was collimated using a set of slits with a rectangular opening of 3×3 cm^2, placed at a distance of 47.18 m from the cold source. The I-BM was placed at a distance 47.42 m from the cold source. A reference Eurisys Mesures ^{3}He beam monitor was placed downstream of the I-BM at a distance of 50.36 m from the cold source.

5 Results

Figure 6 shows the raw signal from the I-BM recorded for the highest achievable flux on V20 (ca. 3×10^6 n/s/cm^2 or 1.9×10^6 n per pulse). The frequency of time stamping was set as 800 ns (there are 100 values/bins stored every 80 ms). The flux was high enough to distinguish one pulse from another directly, without the necessity of averaging over time. The expected 71.4 ms pulse length is depicted in the bottom figure. This is an important result, concluding that the single neutron pulse measurement is absolutely possible when having a neutron beam with high intensity.
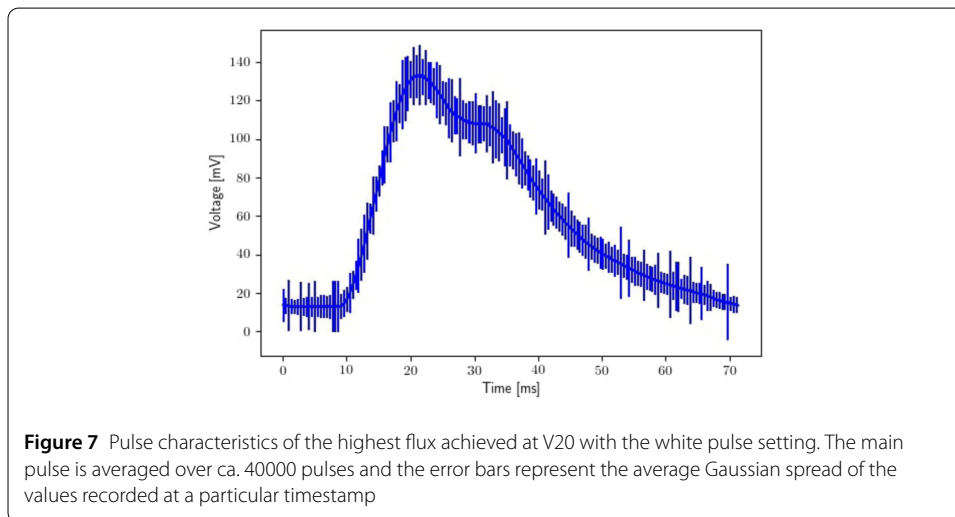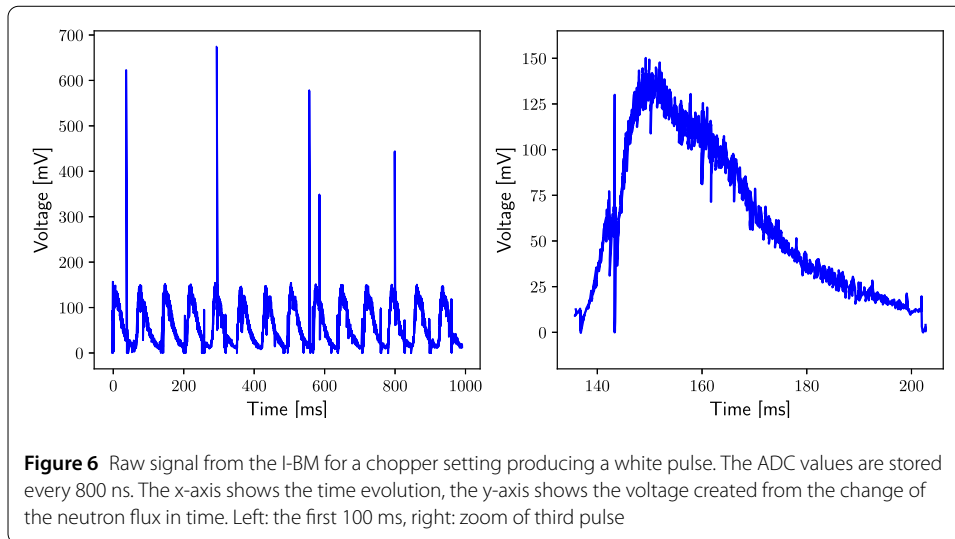
Figure 7 is recorded for the same chopper settings as Fig. 6. It depicts the individual neutron pulses summed and averaged over time. Here, the sharp spikes (an example of which can be seen in the raw signals of Fig. 6, where 5 peaks reach values higher than 300 mV) are filtered away. The uncertainties represent the $\pm\sigma$, where σ is the coefficient of the Gaussian fitting the distribution of the summed and averaged signals recorded at a particular time bin in the pulse.

Similarly, Fig. 8 shows an average pulse with error bars of $\pm\sigma$, where σ is the fitting coefficient in Gaussian distribution of the signals recorded at a particular time bin in the 3Å pulse setting. In this occasion the signal is 20 times weaker as the choppers select only a part of the previously shown white pulse, but still clearly visible when averaged over time.

Further investigations on the signal disturbances that compromised the data taken on the beam time revealed three fold sources that could meanwhile be successfully addressed:

1. high voltage discharges on internal corners

Figure 6 Raw signal from the I-BM for a chopper setting producing a white pulse. The ADC values are stored every 800 ns. The x-axis shows the time evolution, the y-axis shows the voltage created from the change of the neutron flux in time. Left: the first 100 ms, right: zoom of third pulse

Figure 7 Pulse characteristics of the highest flux achieved at V20 with the white pulse setting. The main pulse is averaged over ca. 40000 pulses and the error bars represent the average Gaussian spread of the values recorded at a particular timestamp
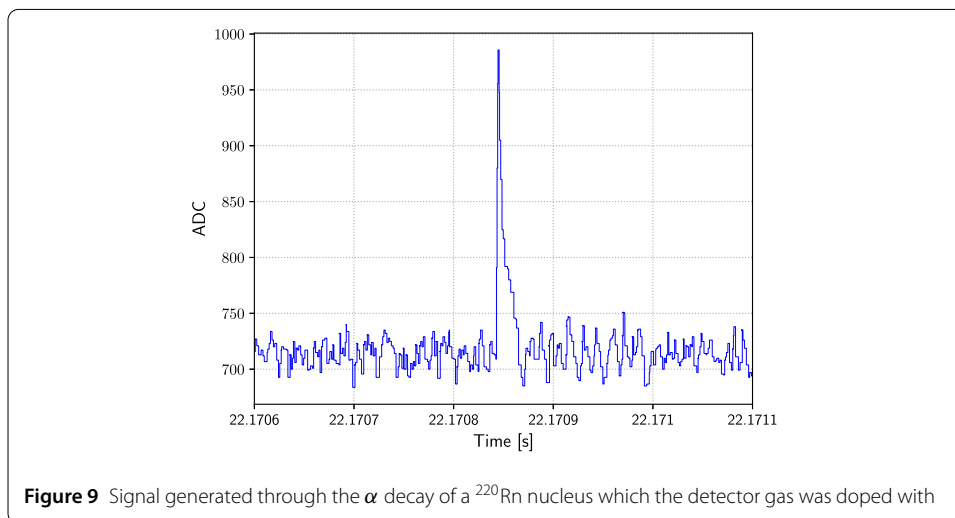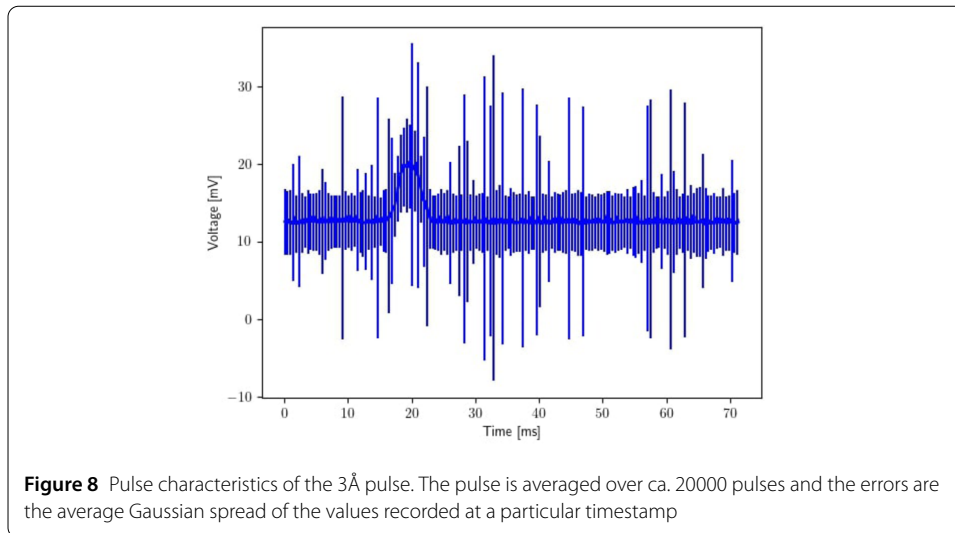
2. dust in the chamber that toggles upon biasing from one electrode to the other
3. residual switch mode power supply disturbances.

Signal quality in this precision measurement could now be improved such that even individual neutron conversions may clearly be distinguished in the recorded current signal. As an example, Fig. 9 shows the signal generated through the alpha-decay of a ^{220}Rn nucleus which the detector gas had been doped with. This signal may be higher than the signal of a converted neutron though it is similarly limited by the chamber's gap width of 2 mm. Under the same operating conditions, Fig. 10 shows how stable the device can be operated when high voltage discharges and dust in the chamber are avoided.

Figure 11 shows the white pulse measurement transformed for comparison to reference data. The raw ADC data are summed and averaged over time, as in Fig. 7. The voltage is converted to intensity according to Eq. (2), the measured TOF is converted to wavelength λ based on the monitor distance from the cold source and the raw λ spectrum is then corrected with the wavelength-dependent monitor efficiency (see Fig. 4). The three distributions represent the intensity recorded with the I-BM, the intensity recorded at the same
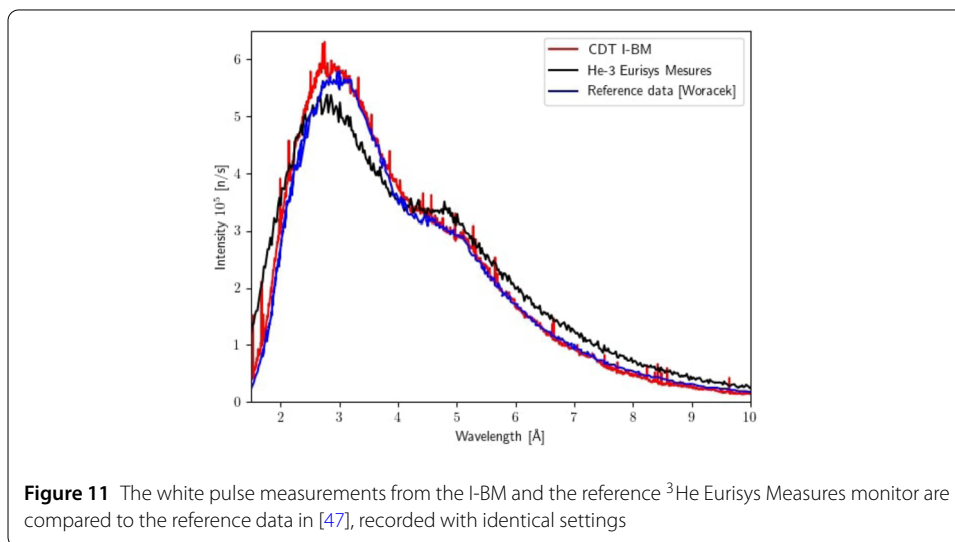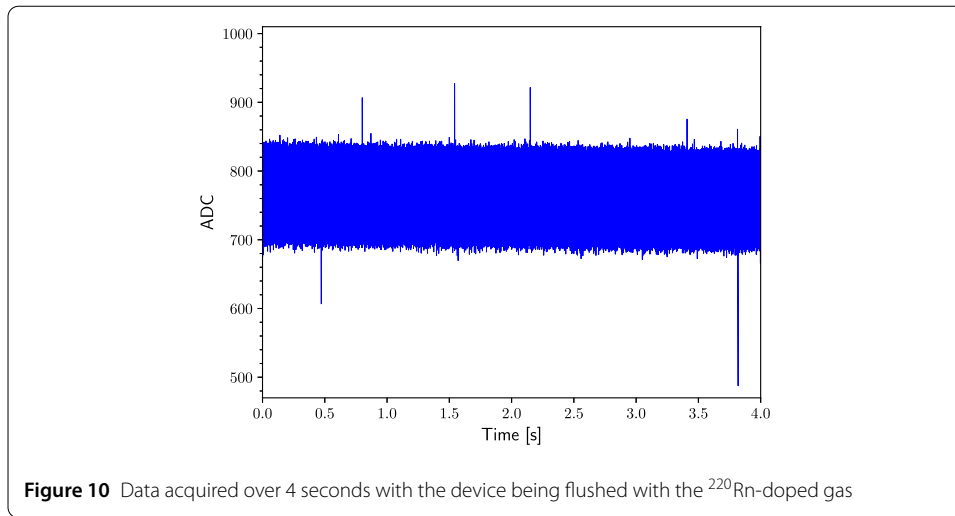
Figure 8 Pulse characteristics of the 3Å pulse. The pulse is averaged over ca. 20000 pulses and the errors are the average Gaussian spread of the values recorded at a particular timestamp

Figure 9 Signal generated through the α decay of a ^{220}Rn nucleus which the detector gas was doped with

time further downstream with the ^{3}He Eurisys Mesures and the reference measurement reported in [47]. The I-BM measurement appears to match well the one from [47]. The ^{3}He Eurisys Mesures monitor peaks at a lower maximum than the other two distributions and the shape of the pulse is broader. This is due to its position further downstream, where neutrons are expected to have spread broader in TOF [1]. The integrated pulse between the two differs by 10%.
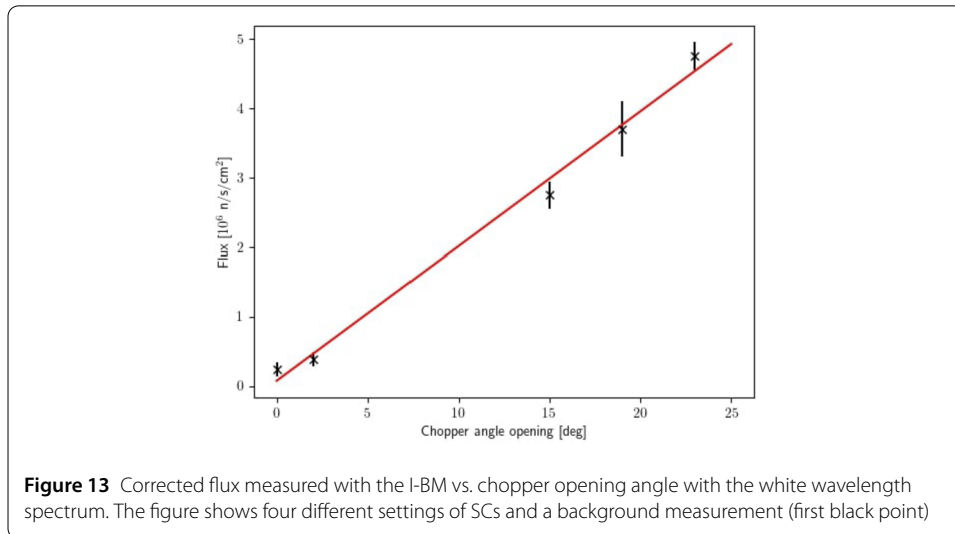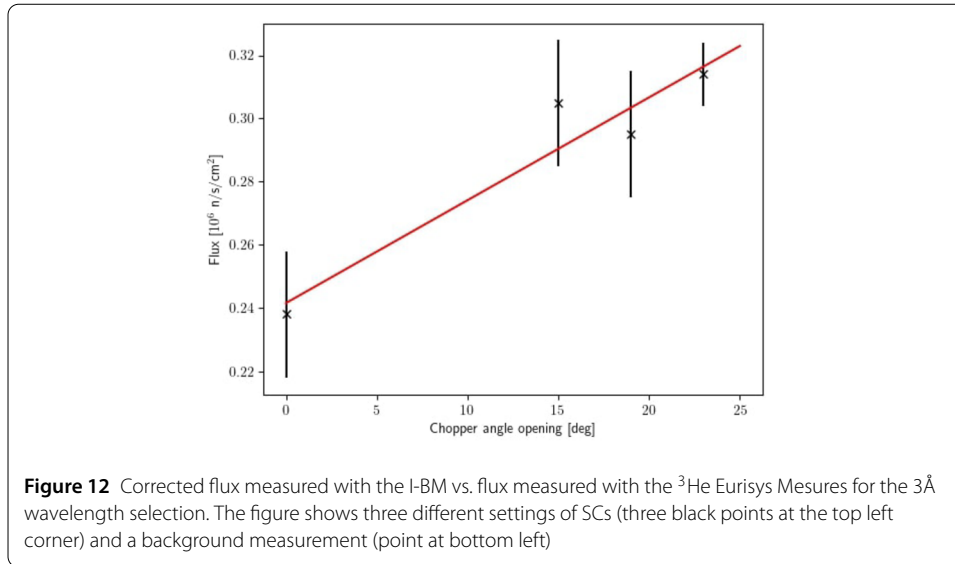
5.1 Performance evaluation with the 3Å pulse

Figure 12 shows the efficiency-corrected integral of the pulse shown in Fig. 8 for three different settings of the SCs (varying intensity). The chopper settings are such that allow the flux to increase linearly as the chopper angle opening between the two SC disks increases (see for example measurements performed earlier at V20 [3]). Additionally, a point close to 0 shows the electronic background. The respective measurement was taken with the neutron beam off. The device produces a continuous line of current even when exposed to no neutrons which is due to the baseline electronics noise.

Figure 10 Data acquired over 4 seconds with the device being flushed with the ^{220}Rn-doped gas

Figure 11 The white pulse measurements from the I-BM and the reference ^{3}He Eurisys Measures monitor are compared to the reference data in [47], recorded with identical settings

The flux uncertainty is calculated from the stability of the measurements over time, i.e. the measurements were taken for a period of time from which the total number of counts for each minute was measured and an average uncertainty was calculated. The linear fit demonstrates the linearity of the monitor response in the measured flux range. This shows sensitivity of the monitor down to fluxes as low as 10^3 n/s/cm^2.

5.2 Performance evaluation with the white pulse

Figure 13 shows the efficiency-corrected integral of the 71.4 ms long pulse (as in Fig. 11) for various settings of the SCs. The flux uncertainty is calculated from the measurements taken for a period of time from which the total number of counts for each minute was measured and an average error was calculated, just like in the 3Å case. The uncertainties are significantly lower than before. The flux is approximately 2 orders of magnitude higher for the white pulse (when leaving the WB chopper open) and the electronic background noise contributes a lesser fraction to the measured value. The relationship is clearly linear and due to the low flux uncertainties, the monitor demonstrates a very stable behaviour over time.

Figure 12 Corrected flux measured with the I-BM vs. flux measured with the ^{3}He Eurisys Mesures for the 3Å wavelength selection. The figure shows three different settings of SCs (three black points at the top left corner) and a background measurement (point at bottom left)

Figure 13 Corrected flux measured with the I-BM vs. chopper opening angle with the white wavelength spectrum. The figure shows four different settings of SCs and a background measurement (first black point)

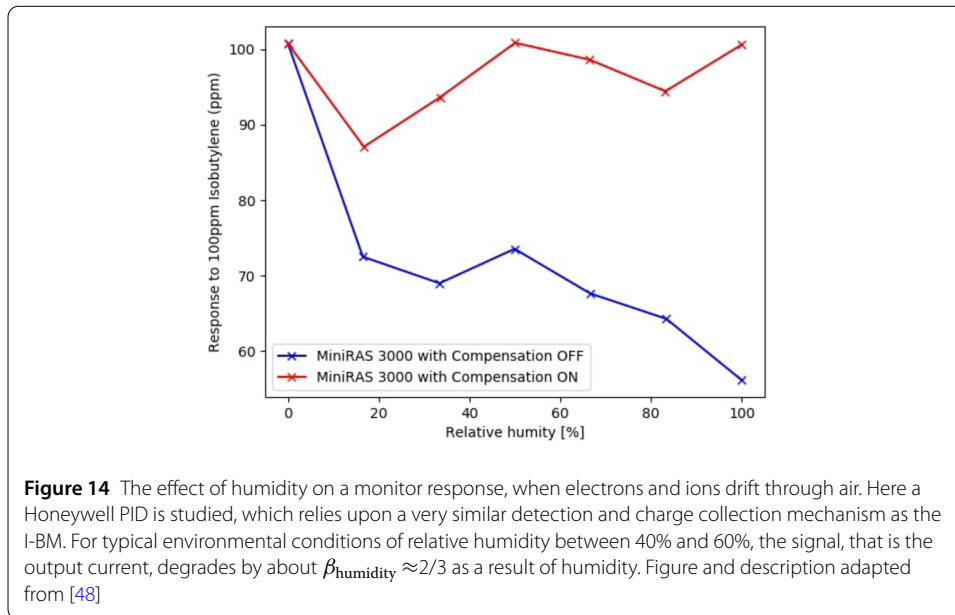## 6 Design for high flux environment

The I-BM response is highly adjustable by varying parameters, such as the thickness of boron coating, the choice of converter, the electronics design and the possibility for anode segmentation. The biggest challenge of utilising the monitor inside the ESS bunker is the expectancy of neutron intensities in the order of 10^{14} n/s for a 2.86 ms long pulse repeating every 71.4 ms, which translates to a maximum $\Phi_{\text{average}} \approx 10^9$ n/s/cm^2.

By using a 100 nm thick boron coating, Eq. (2) can be rewritten as follows:

$$\Phi_c = \frac{I_{\text{monitor}}}{Q_0 \epsilon_n \cdot \frac{2}{3}} = 3.8 \cdot 10^{17} \frac{1}{s} I_{\text{monitor}}[A] \tag{3}$$

$$= 1.3 \cdot 10^{11} \frac{1}{s} U_{\text{out-TIA}}[V]. \tag{4}$$

Such an adjustment of the boron coating thickness would then result in 15 μA of current corresponding to 90 V of dynamical range for a flux as high as 10^{11} n/s/cm^2. The flux upper

Figure 14 The effect of humidity on a monitor response, when electrons and ions drift through air. Here a Honeywell PID is studied, which relies upon a very similar detection and charge collection mechanism as the I-BM. For typical environmental conditions of relative humidity between 40% and 60%, the signal, that is the output current, degrades by about $\beta_{\text{humidity}} \approx 2/3$ as a result of humidity. Figure and description adapted from [48]

range could be further increased by modification of the feedback resistance R_f. The noise performance of the TIA is optimised through the choice of the input amplifier, feedback resistor, input capacitance (sensor and cable) and compensation capacitance. In effect, the amplifier output noise is constant at constant bandwidth, where the bandwidth is determined by the RC of the feedback resistor and the compensation capacitor, which again is directly proportional to the input capacitance R_f. Furthermore, for the bunker location a long cable from the monitor to the TIA might be needed. In order to keep the signal-to-noise ratio low, the electronics need to be adjusted as well, as long cables introduce large input capacitance to the electronics, hence the R_f needs to be adjusted for this reason as well.

If the I-BM is an option to be considered also to monitor flux downstrean of choppers, the converter thickness might be thicker than 100 nm, depending on the anticipated flux at location. High flux capability always introduces low sensitivity and therefore a condition on the lowest measurable flux. Another challenge to consider these monitors for chopper locations is related to the time resolution of the I-BM; in principle the monitor is able to record a value every 100 ns, however reasonable statistics are necessary to be able to see the pulse.

The tested I-BM model operates with air. Ar/CO_2 and possibly N_2 or dry air could be considered, in order to achieve higher stability and smaller deviations in flux measurements. Increasing and decreasing humidity around a beam line can also introduce a factor on the monitor calibration (see Fig. 14 adapted from technical report of CDT [48]). Furthermore, if the spatial distribution of the beam is of importance, the possibility of anode segmentation could be introduced.

7 Conclusions

A prototype thermal neutron beam monitor based on ionisation chamber principles and a boron converter was designed by CDT CASCADE Detector Technologies GmbH and ESS. The performance of this prototype was investigated at the V20 neutron beam line at HZB,

Berlin. The I-BM demonstrated good linearity for various flux ranges, timing capability and sensitivity to neutrons within the range of 0.6-10Å.

The linearity was demonstrated for a 3Å pulse in the flux range of $2\text{-}3\times10^5$ n/s/cm^2 and a white pulse in the range of of $1\text{-}5\times10^6$ n/s/cm^2. The TOF capability for the counter-rotation SC settings resembled the ESS pulse previously recorded and for both the 3Å and the white pulse selection the recorded pulse resembled the pulse recorded simultaneously on a reference ^{3}He Eurisys Mesures beam monitor. Proving that the concept is viable, a further investigation suitable for ESS usage is in preparation in order to be able to facilitate fluxes as high as 10^{12} n/s/cm^2. Aside of ESS, the highly adjustable prototype is expected to be appropriate for many time-resolved measurements for neutron beam fluxes.

In conclusion, the I-BM with the current design and modification of boron coating is fully suitable to be used in the ESS bunker. With further modifications, this monitor could also be a candidate to monitor fluxes in the close proximity of the choppers, in order to diagnose the chopper function, energy distribution of the neutrons and possibly spatial distribution. The design has meanwhile advanced to fit the allocated space envelopes at the ESS beam lines. These monitors will be a central part of the ESS neutron beam monitoring suite.

Declarations

Consent for publication
All authors have agreed to the publication of this paper.

Competing interests
The authors declare that they have no competing interests.

Author contribution
VM tested the monitor with MK's support. She analysed the data and authored the manuscript. KK and RH-W guided the data analysis, structured the narrative and finalised the paper. CS, MK produced the monitor that was co-developed with RH-W. PK supported the measurements at the V20 beamline in Berlin. AL produced the mechanical supports for the monitor tests. All authors read and approved the final manuscript.

Author details
[1]European Spallation Source ERIC, 22100, Lund, Sweden. [2]Division of Nuclear Physics, Lund University, 223 63, Lund, Sweden. [3]CERN, 1211, Geneva, Switzerland. [4]University of Hamburg, 20146, Hamburg, Germany. [5]CDT CASCADE Detector Technologies GmbH, 69123, Heidelberg, Germany. [6]GSI Helmholtzzentrum für Schwerionenforschung GmbH, 64291, Darmstadt, Germany. [7]Università degli Studi di Milano-Bicocca, 20126, Milano, Italy. [8]University of Glasgow, G12 8Q, Glasgow, United Kingdom. [9]Sensors and Devices Centre, Foundation Bruno Kessler, 38123, Trento, Italy. [10]*Present address:* RISE, 1040, Vienna, Austria.

Publisher's Note

Springer Nature remains neutral with regard to jurisdictional claims in published maps and institutional affiliations.

References
1. Maulerova V et al. First neutron data recorded at the V20 test instrument utilizing prototype chopper systems and beam monitors planned for ESS. EPL. 2019;128(5):52001. https://doi.org/10.1209/0295-5075/128/52001.

2. Issa F, Khaplanov A, Hall-Wilton R, Llamas I, Dalseth Riktor M, Brattheim SR, Perrey H. Characterization of thermal neutron beam monitors. Phys Rev Accel Beams. 2017;20:092801. https://doi.org/10.1103/PhysRevAccelBeams.20.092801.

3. Maulerova V, Kanaki K, Kadletz PM, Woracek R, Wilpert T, Fissum K, Laloni A, Mauritzson N, Issa F, Hall-Wilton R. Vanadium-based neutron beam monitor. Phys Rev Accel Beams. 2020;23:072901. https://doi.org/10.1103/PhysRevAccelBeams.23.072901.

4. Neutron Data Booklet. Institut Laue-Langevin. https://www.ill.eu/fileadmin/user_upload/ILL/1_About_ILL/Documentation/NeutronDataBooklet.pdf (2003)

5. Wolff MM, Stephens WE. A pulsed mass spectrometer with time dispersion. Rev Sci Instrum. 1953;24:616. https://doi.org/10.1063/1.1770801

6. Nonato FBC et al. Characterization tests of a new parallel plate ionization chamber for use in electron beams. Radiat Phys Chem. 2014;104:244. https://doi.org/10.1016/j.radphyschem.2014.06.011

7. Medin J, Andreo P, Grusell E, Mattsson O, Montelius A, Roos M. Ionization chamber dosimetry of proton beams using cylindrical and plane parallel chambers. N_W versus N_K chamber calibrations. Phys Med Biol. 1995;40:1161. https://doi.org/10.1088/0031-9155/40/7/002

8. Tchelidze L, Hassanzadegan H, Jarosz M, Jansson A. Beam loss monitoring at the European Spallation Source. In: Proceedings of IBIC2013. Oxford, UK. 2013.

9. Kittelmann ID, Shea T. Simulations and detector technologies for the beam loss monitoring system at the ESS LINAC. In: Proceedings of HB2016. Malmö, Sweden. 2016.

10. Peggs S, et al. *European Spallation Source Technical Design Report ESS-2013-001*. http://eval.esss.lu.se/cgi-bin/public/DocDB/ShowDocument?docid=274 (2013)

11. Garoby R et al. The European Spallation Source Design. Phys Scr. 2017;93:014001. https://doi.org/10.1088/1402-4896/aa9bff

12. ESS website. https://europeanspallationsource.se/. Accessed: 2022-01-25

13. Andersen KH et al. The instrument suite of the European Spallation Source. Nucl Instrum Meth A. 2020;957:163402. https://doi.org/10.1016/j.nima.2020.163402.

14. Mezei F, Russina M. Neutron-optical component array for the specific spectral shaping of neutron beams or pulses. patent: US20050157831A1 ESS-0502620 (2006)

15. Andersen KH, Bertelsen M, Zanini L, Klinkby EB, Schönfeldt T, Bentley PM, Saroun J. Optimization of moderators and beam extraction at the ESS. J Appl Crystallogr. 2018;51:264. https://doi.org/10.1107/S1600576718002406.

16. Fernandez-Alonso F, Price DL. Neutron scattering—applications in biology, chemistry, and materials science. Amsterdam: Elsevier; 2017.

17. Staron P, Schreyer A, Clemens H, Mayer S. Neutrons and synchrotron radiation in engineering materials science: from fundamentals to applications. 2nd ed. New York: Wiley; 2017. https://doi.org/10.1002/9783527684489.

18. Kardjilov N, Manke I, Woracek R, Hilger A, Banhart J. Advances in neutron imaging. Mater Today. 2018;21:652. https://doi.org/10.1016/j.mattod.2018.03.001.

19. Winkler B. Applications of neutron radiography and neutron tomography. Rev Mineral Geochem. 2006;63:459. https://doi.org/10.2138/rmg.2006.63.17.

20. Bentley PM. Instrument suite cost optimisation in a science megaproject. J Phys Commun. 2020;4:045014. https://doi.org/10.1088/2399-6528/ab8a06.

21. LND: Fission chamber. https://www.lndinc.com/products/neutron-detectors/3053/. Accessed: 2022-01-25

22. Croci G, Cazzaniga C, Claps G, Tardocchi M, Rebai M, Murtas F, Vassallo E, Caniello R, Cippo EP, Grosso G, Rigato V, Gorini G. Characterization of a thermal neutron beam monitor based on gas electron multiplier technology. Prog Theor Exp Phys. 2014;2014:083H01. https://doi.org/10.1093/ptep/ptu105.

23. Croci G, Claps G, Caniello R, Cazzaniga C, Grosso G, Murtas F, Tardocchi M, Vassallo E, Gorini G, Horstmann C, Kampmann R, Nowak G, Stoermer M. GEM-based thermal neutron beam monitors for spallation sources. Nucl Instrum Meth A. 2013;732:217. https://doi.org/10.1016/j.nima.2013.05.111.

24. Cancelli S, Muraro A, Cippo EP, Romanelli G, Abba A, Chen Y, Grosso G, Gorini G, Hu Z, Lai C-C, Cormack OM, Robinson L, Svensson P-O, Tardocchi M, Hall-Wilton R, Xie Y, Zhijia S, Zhou J, Zhou X, Croci G. Development of a ceramic double thick GEM detector for transmission measurements at the VESUVIO instrument at ISIS. JINST. 2021;16:06003. https://doi.org/10.1088/1748-0221/16/06/P06003.

25. Issa F, Hall-Wilton R, Quintanilla A, Olsson M, Zielinski D, Kanaki K, Tsapatsaris N. Parasitic neutron beam monitoring: proof of concept on gamma monitoring of neutron chopper phases. EPL. 2020;132:22001. https://doi.org/10.1209/0295-5075/132/22001.

26. Ohshita H, Uno S et al. Development of a neutron detector with a GEM. Nucl Instrum Meth A. 2010;623:126. https://doi.org/10.1016/j.nima.2010.02.170.

27. Zhou J et al. A ceramic GEM-based neutron beam monitor for China Spallation Neutron Source. Nucl Instrum Meth A. 2020;962:163593. https://doi.org/10.1016/j.nima.2020.163593.

28. Fermi E, Marshall J, Marshall L. A thermal neutron velocity selector and its application to the measurement of the cross section of boron. Phys Rev. 1953;72:193. https://doi.org/10.1103/PhysRev.72.193.

29. Evans L, Bryant P. LHC machine. JINST. 2008;3:08001. https://doi.org/10.1088/1748-0221/3/08/S08001.

30. Dehning B. *Beam loss monitor system for machine protection, CERN-AB-2005-062* (2005)

31. Dehning B. Beam loss monitors at LHC. In: 2014 joint international accelerator school: beam loss and accelerator protection. 2016. p. 303. https://doi.org/10.5170/CERN-2016-002.303.

32. Hall-Wilton RJ, Macina D, Talanov V. Recommended locations of beam loss monitors for the ATLAS Roman Pots, CERN-LHC-PROJECT-NOTE-397, CERN-TS-NOTE-2007-003 (2007)

33. Appleby RB, Macina D, Talanov V, Hall-Wilton R. Expected Performance of TOTEM BLMS at the LHC, CERN-ATS-2009-124 (2009)

34. Müller S. The Beam Condition Monitor 2 and the Radiation Environment of the CMS Detector at the LHC. PhD thesis, Karlsruhe U. (2010). https://doi.org/10.5445/IR/1000022456

35. Fricke H, Hart E. Chemical dosimetry in book, ionizing radiation dosimetry. 2: instrumentation. New York: Academic Press; 1966.

36. Müller S, deBoer W, Schneider M, Sabellek A, Schmanau M, Ruhle C, Schneider T, Hall-Wilton R. Study of leakage currents in pCVD diamonds as function of the magnetic field. Phys Status Solidi A. 2009;206:2091. https://doi.org/10.1002/pssa.200982221.

37. Segui L, Alves H, Aune S, Beltramelli J, Bertrand Q, Combet M, Dano-Daguze A, Desforge D, Dolenc Kittelmann I, Gougnaud F, Joannem T, Kebbiri M, Lahonde-Hamdoun C, Le Bourlout P, Legou P, Maillard O, Marcel A, Mariette Y, Marroncle J, Nadot V, Papaevangelou T, Shea T, Tsiledakis G. Characterization and first beam loss detection with one ESS-nBLM system detector. In: Proceedings of the 8th international beam instrumentation conference IBIC2019. 2019. p. 29. https://doi.org/10.18429/JACoW-IBIC2019-MOBO04.

38. Papaevangelou T et al. ESS nBLM: beam loss monitors based on fast neutron detection. In: 61st ICFA advanced beam dynamics workshop on high-intensity and high-brightness hadron beams. 2018. p. 1–4. https://doi.org/10.18429/JACoW-HB2018-THA1WE04.

39. Dolenc Kittelmann I, Alves F, Bergman E, Bertrand Q, Cichalewski W, Derrez C, Grishin V, Jabłoński G, Jałmużna W, Joannem T, Kiełbik R, Legou P, Mariette Y, Nadot V, Papaevangelou T, Rosengren K, Segui L, Shea T. Neutron sensitive beam loss monitoring system for the ess linac. In: Proceedings of the 8th international beam instrumentation conference IBIC2019. 2019. https://doi.org/10.18429/JACoW-IBIC2019-MOPP022.

40. Jabłoński G, Kittelmann ID, Jałmużna W, Kiełbik R, Cichalewski W, Rosengren K, Shea T, Santos Alves F, Grishin V, Papaevangelou T, Segui L, Zamantzas C. FPGA-based data processing in the neutron-sensitive beam loss monitoring system for the ESS linac. In: 2019 MIXDES—26th international conference "mixed design of integrated circuits and systems". 2019. p. 101. https://doi.org/10.23919/MIXDES.2019.8787166.

41. Iijima K, Sanami T, Hagiwara M, Saito K, Sasaki S. Development of a current-readout type neutron monitor for burst neutron fields. Nucl Sci Technol. 2011;2011:300–3. https://doi.org/10.15669/pnst.1.300.

42. Gledenov YM, Salatski VI, Sedyshev PV. The ^{14}N(n,p)^{14}C reaction cross section for thermal neutrons. Z Phys Hadrons Nucl. 1993;346:307. https://doi.org/10.1007/BF01292522.

43. International Evaluation of Neutron Cross-Section Standards, IAEA (2007), ISBN:92-0-100807-4. Non-serial Publications

44. Piscitelli F. Boron-10 layers, neutron reflectometry and thermal neutron gaseous detectors. PhD thesis, University of Perugia, Italy. https://jinst.sissa.it/jinst/theses/2021_JINST_TH_001.jsp (2014)

45. Basañez AC, Kanaki K, Piscitelli F. DECal, a Python tool for the efficiency calculation of thermal neutron detectors based on thin-film converters. arXiv:1801.07124 (2018)

46. Strobl M, Bulat M, Habicht K. The wavelength frame multiplication chopper system for the ESS test beamline at the BER II reactor—a concept study of a fundamental ESS instrument principle. Nucl Instrum Meth A. 2013;705:74. https://doi.org/10.1016/j.nima.2012.11.190.

47. Woracek R, Hofmann T, Bulat M, Sales M, Habicht K, Andersen K, Strobl M. The test beamline of the European Spallation Source—instrumentation development and wavelength frame multiplication. Nucl Instrum Meth A. 2016;839:102. https://doi.org/10.1016/j.nima.2016.09.034.

48. Schmidt CJ. The Ionization-Chamber beam monitor I-BM for thermal and cold neutron beams. Technical report, CDT CASCADE Detector Technologies GmbH. https://n-cdt.com/wp-content/uploads/2019/09/Documentation-Ionization-Chamber-I-BM-Final-12.12.16.pdf (2016)